Available online at www.sciencedirect.com

ScienceDirect

Procedia CIRP 82 (2019) 26–31

www.elsevier.com/locate/procedia

17th CIRP Conference on Modelling of Machining Operations

Revisiting flow stress modelling for simulating chip formation of carbon and low alloy steels

Thomas H. C. Childs[a]*

[a]School of Mechanical Engineering, University of Leeds, LS29JT, UK

* Corresponding author. *E-mail address:* t.h.c.childs@leeds.ac.uk

Abstract

In previous papers the present author has successfully predicted chip formation in machining carbon steels with a model that supposes all carbon steels to have the same flow stress thermal softening and a temperature independent strain rate hardening but to be characterized by individual strain hardening behaviours. It has been necessary to suppose thermal softening to be shifted to higher temperatures than observed experimentally. It is now found alternatively that the thermal softening shift is not required if it is supposed that the strain rate hardening increases slightly in proportion to temperature at temperatures greater than 600°C. The new model results are illustrated and compared to experiment for the low alloy steel BS970:708M40. The relation between flow stress and friction modelling is also discussed.

Peer-review under responsibility of the scientific committee of The 17th CIRP Conference on Modelling of Machining Operations

Keywords: Cutting; Chip formation; Friction modelling

1. Introduction

In a previous series of papers [1-4] the present author has developed a flow stress model for annealed carbon and low alloy steels. Its use in simulations of metal cutting in general engineering conditions, without built up edge formation, leads to successful prediction of cutting forces, chip thickness ratio and temperatures (damage modelling is needed for built up edge prediction). The flow stress model is of product form Eq. 1 (where the symbols have their usual meaning).

$$\bar{\sigma} = f\left(\bar{\varepsilon}\right) g\left(\dot{\bar{\varepsilon}}\right) \Theta\left(T\right) \tag{1}$$

In principle the functions f, g and Θ are independent so may be determined in any convenient conditions, for example f and g may be measured at room temperature and Θ at low strain rate, say 10^{-3}/s. In practice such choices lead to poor predictions of experimental results. However the simple structure of Eq. 1 can be maintained if appropriate choices of conditions and adjustments to measurements are made.

It has been supposed that the functions Θ and g are the same for all the steels (as is revisited in section 2). Differences between the steels then come from their strain hardening but inputting strain hardening measured at room temperature and a strain rate of 10^{-3}/s to simulations does not lead to agreement with observations. At high strain rates steels show an upper yield point, or yield delay [5] that influences chip formation. This was first considered qualitatively by Zorev who stated that steels form thinner chips at high speeds than at low speeds because there is insufficient time for them to deform ahead of the tool [6]. This is approximately accounted for in [1-4] by supposing that the initial yield stress is larger than actually measured at low strain rate while the yield stress at a strain of 1.0 remains unchanged. The increase in the initial yield stress is determined by assuming the measured strain hardening exponent is reduced three-fold (see section 3 for more detail). This is the same change in exponent as found by Oxley in his

2212-8271
Peer-review under responsibility of the scientific committee of The 17th CIRP Conference on Modelling of Machining Operations
10.1016/j.procir.2019.03.222

inverse method of determining flow stress from machining experiments [7].

Thermal softening of steels shows a dynamic strain ageing peak (blue brittleness) in temperature ranges that depend on strain rate. Fig. 1 shows $\Theta(T)$ measured for a 0.35%C steel at strain rates of 0.1 and 450/s [8]. The ageing peak temperature increases from ≈ 400 to 600°C as strain rate increases from 0.1 to 450/s. The peak temperature is not much different at the machining strain rates of 10^3-10^4/s (see section 2) but when $\Theta(T)$ for these strain rates is used in [1-4], poor agreement is again found between prediction and observation. It has been necessary to assume the rapid softening above the ageing peak temperature to be delayed to 900°C, as also shown in Fig. 1. Whether it is physically realistic to delay the softening to above the normal Ac1 temperature for steels, perhaps due to rapid heating rate during metal cutting, has never been clear.

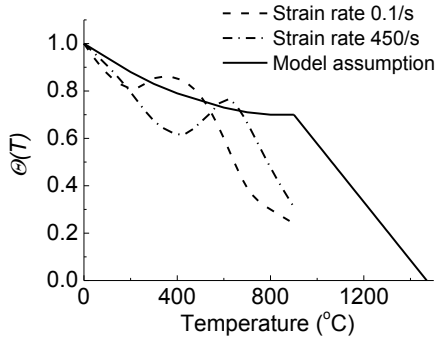

Fig. 1. Example $\Theta(T)$ behaviours: dashed lines measured values at two strain rates for a 0.35%C steel [8], solid line as modelled in [1-4].

The original work here revisits this thermal softening question. New simulations show that it is not necessary to delay the thermal softening. $\Theta(T)$ as measured leads to good predictions of experimental results if, instead, the strain rate hardening, previously measured at room temperature, is assumed to increase with temperature at temperatures > 600°C, by a small amount as is well-known from metal forming conditions [9].

The new approach is illustrated by simulations of chip formation from machining a BS970:708M40 low alloy steel (equivalent to AISI 4340) at uncut chip thickness h = 0.3mm at cutting speeds v_c from 50 to 300m/min, with a tool of rake angle γ = 6°. Fig. 2 shows experimentally determined specific cutting and thrust forces F_C* and F_T* and chip thickness ratio *t/h*, compared to the previously simulated results [4]. They serve as a bench mark against which to judge the new simulations. This steel and its machining conditions are chosen because chip/tool contact temperature measurements, from the tool/work thermocouple method, also exist for further comparisons with simulated results. The experimental data are accurate to ± 5%.

Chip / tool friction must also be modelled. Eq. 2 gives the behaviour assumed here, with τ and σ_n the friction and normal stresses at the contact, μ the friction coefficient and k the local shear flow stress of the chip material, assumed equal to the local $\bar{\sigma}/\sqrt{3}$.

$$\tau = min.\left(\mu\sigma_n, k\right) \tag{2}$$

In this work, μ = 1 always. This ensures that Eq. 2 gives $\tau = k$ over most of the contact. This approach differs from others in which μ varies with cutting conditions, chosen to depend for example on sliding speed [10], temperature [11] or both [12]. The relation between these approaches is discussed, after presentation of the new results in section 4 and discussion of the flow stress modelling in section 5.

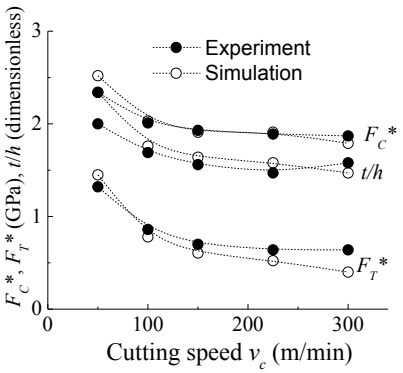

Fig. 2. Experimental and simulated F_C*, F_T* and *t/h*: 708M40 steel, γ = 6°.

2. $\Theta(T)$ and $g\left(\dot{\bar{\varepsilon}}\right)$ for carbon and low alloy steels

The assumed similarity of Θ and g for all annealed carbon and low alloy steels is revisited here, starting from results from a current cooperative action between researchers in The International Academy for Production Engineering (CIRP). This has produced thermal softening and strain rate hardening data for annealed AISI 1045 steel [13]. Figs. 3a and 4a give Θ and g determined by the present author from these data. Θ is stress at temperature relative to stress at room temperature determined at strain rates from 2000 to 6000/s by Hopkinson bar tests. Fig. 3a's results are for three levels of strain, from 0.05 to 0.45, after correcting temperatures to allow for adiabatic heating. g is the stress at strain rate relative to the stress at a strain rate 10^{-3}/s determined by screw, drop hammer and Hopkinson bar machines at room temperature to avoid strain ageing, and a strain of 0.05 to avoid heating effects.

The results of Fig. 3a may be fitted to a superposition of a curve continuously decreasing with increasing temperature and a curve peaking at 650°C, as in Eq. 3. The coefficient a defines the height of the peak. a = 0.25 for the fitting line in the figure. The Fig. 4a results may be fitted to a power law, as in Eq. 4. m_0 = 0.03 and 0.04 for the upper and lower fitting lines. Many other functional ways to fit the data are to be found in the literature, both phenomenological and physically based. The present choices are simple ones.

$$\Theta(T) = 1 - 0.00091T + 1.56\times10^{-7}T^2 + a\,exp\left[-6.5\times10^{-5}\left(T - 650^2\right)\right] \tag{3}$$

$$g\left(\dot{\bar{\varepsilon}}\right) = \left(1 + \dot{\bar{\varepsilon}}\right)^{m_0} \tag{4}$$

The present results are compared to pre-existing ones in the literature in Figs. 3b and 4b. In both cases the solid lines are the fitting lines from Figs. 3a and 4a. Fig. 3a contains results from [8] for pure Fe and 0.15, 0.35, 0.45 and 0.55C steels. Variations between them are < ± 10%; Fig. 3a shows the mean

values. It also contains results for a 0.18C steel [14], a 708M40 steel [15] and a 0.75C (eutectic) steel [16]: all these data are from rapidly pre-heated Hopkinson bar tests. Finally another 0.45C steel result is added [17]. These are the evidence for Θ not varying between annealed steels, though there is large scatter around the size and position of the ageing peak that will be considered further in section 5. (Johnson and Cook also observed the ageing peak but ignored it for fitting to their softening equation [18].)

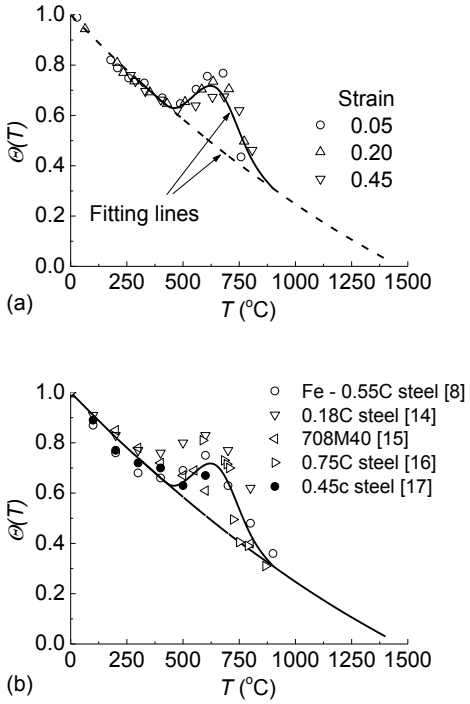

Fig. 3. $\Theta(T)$ determined (a) for an annealed 0.45C steel [13] compared to (b) other results derived from the literature.

In Fig. 4b a large number of pre-existing results match those in Fig. 4a: these include previous work on AISI 1045 [19], Johnson's and Cook's original results for AISI 4340 extracted from the raw data in [18] and results for the equivalent steel 708M40 [15], as well as for a 0.25%C steel [20]. However there are also significant departures from the Fig. 4a bounds. The figure includes, as the dashed lines, the Eq. 4 curves for m_0 = 0.08, 0.06 and 0.02. The Johnson and Cook results for ARMCO iron, again from [18], follow the m_0 = 0.08 line; a review of early work on mild steels has results that follow m_0 = 0.06 [21]. It is not safe to assume g to be the same for all steels though m_0 = 0.03 to 0.04 for many cases, including that followed up here.

(m_0 reduces with increasing hardness of the steel, for the same reason and equivalently as the strain rate coefficient C in the Johnson-Cook law reduces with increasing hardness. The increase in flow stress as strain rate increases from 10^{-3} to 10^{+3}/s at room temperature is similar for all the steels, at ≈ 200 to 250MPa, whatever value the yield stress has at the strain rate 10^{-3}/s, based on [22]. Then g, which is the ratio of the high to low strain rate yield stress reduces as the low strain rate yield stress increases.)

This section's review gives a justification for applying the thermal softening and strain rate hardening Eqs. 3 and 4, with their coefficients obtained from tests on AISI 1045, to simulating chip formation of BS970:708M40.

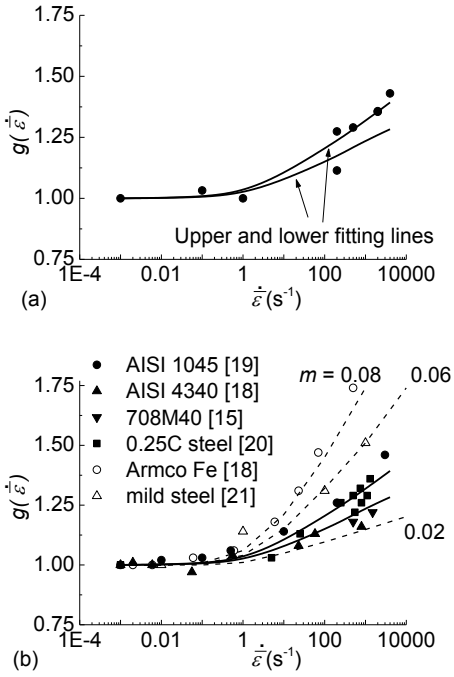

Fig. 4. $g\left(\dot{\bar{\varepsilon}}\right)$ determined (a) for an annealed 0.45C steel [13] compared to (b) other results derived from the literature.

3. Simulation conditions

Simulations of machining BS970:708M40 steel have been carried out with the commercial code AdvantEdge-2D v7.4, with the thermal softening flow stress model of Eq. 3 with a = 0.25 and the strain rate hardening model of Eq. 4 with m_0 = 0.03 and 0.04. The Eq. 4 behaviour has also been augmented in the manner of Eq. 5, with m_T = 0.0002 and T_{crit} = 600°C, i.e. half the melting temperature (K).

$$m = m_0 + m_T\left(T - T_{crit}\right), \quad T > T_{crit} \tag{5}$$

Strain hardening, measured at room temperature and quasi-statically is taken from [4] to follow Eq. 6, with ε_c = 1.0. The as-measured coefficients are σ_0 = 765MPa, ε_0 = 0.0094 and n = 0.083. The coefficients as-modified for yield delay (see section 1) are σ_0 = 990MPa, ε_0 = 0.0094 and n = 0.028

$$\begin{aligned} f\left(\bar{\varepsilon}\right) &= \sigma_0\left(1+\bar{\varepsilon}/\varepsilon_0\right)^n, \quad \bar{\varepsilon} \le \varepsilon_c \\ &= \sigma_0\left(1+\varepsilon_c/\varepsilon_0\right)^n, \quad \bar{\varepsilon} > \varepsilon_c \end{aligned} \tag{6}$$

Three sets of simulation results are presented in Section 4: (i) with as-measured strain hardening, Eq. 3 thermal softening (a = 0.25) and Eq. 4 strain rate hardening (m_0 = 0.04); (ii) as (i) except as-modified strain hardening; (iii) as (ii) except Eq. 5 strain rate hardening (m_0 = 0.03 and 0.04, m_T = 0.0002).

In all cases the work thermal conductivity, specific heat and density are taken to be 39W/m°C, 570J/kg°C and 7860 kg/m^3. The tool thermal conductivity is taken as 40W/m°C and its cutting edge radius as 20μm. Minimum mesh size is 5μm.

4. Results

The three sets of simulation results are in Figs. 5-7. With as-measured strain hardening (Fig. 5) there is agreement between measured and simulated F_C* and *t/h* but simulations underestimate F_T*. Modifying strain hardening (Fig. 6) results in the simulations underestimating all of F_C*, F_T* and *t/h*, systematically. Simulations and experiments are brought back approximately into agreement by assuming the strain rate hardening exponent *m* to increase with temperature at temperatures above half the melting point (Fig. 7). In this case, the simulations with m_0 = 0.03 and 0.04 span the experimental F_C* and both slightly underestimate F_T* and *t/h*. Overall agreement is similar to that previously found by delaying thermal softening (Fig. 2).

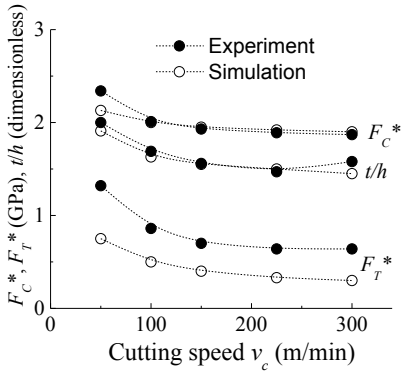

Fig. 5. Experimental and simulated F_C*, F_T* and *t/h*, with the as-measured flow stress input to the simulations.

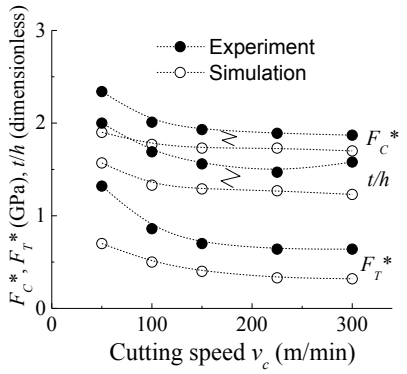

Fig. 6. Experimental and simulated F_C*, F_T* and *t/h*, with the as-modified strain hardening flow stress input to the simulations.

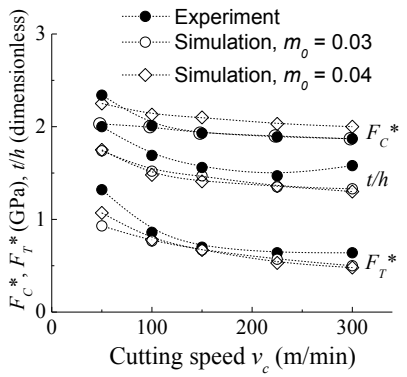

Fig. 7. Experimental and simulated F_C*, F_T* and *t/h*, with the as-modified strain hardening and augmented strain rate hardening flow stress input to the simulations.

A similar agreement between the effects of enhancing strain rate hardening and delaying thermal softening is found for the predicted average temperature rise over the chip / tool contact. Fig. 8 shows that both give agreement with measurements from the chip / tool thermocouple method [4].

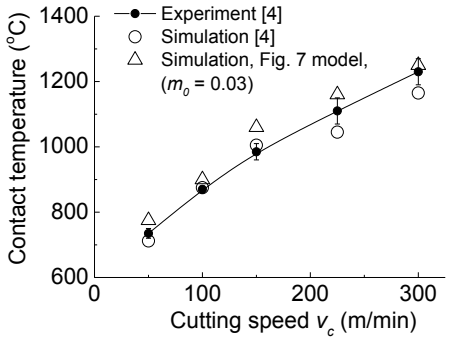

Fig. 8. Experimental and simulated average chip / tool contact temperature.

5. Discussion

5.1. Flow stress modelling

Section 2's review shows that the previous assumption that all steels can be treated as having the same values of $g\left(\dot{\bar{\varepsilon}}\right)$ and *Θ(T)* is over-simple. The softest steels (mild steel, also iron) have appreciably larger strain rate hardening exponents *m* than other steels, as a consequence of the chosen product form, Eq. 1, rather than an additive form, as [22], of flow stress model. However many steels have *m* values in the range 0.03 to 0.04 (Fig. 4b). The sensitivity of cutting forces and chip thickness ratio to changes in *m* in this range is not very high (Fig. 7).

Of more concern is the wide scatter in *Θ(T)* in the blue-brittle temperature range of 500-700°C (Fig. 3b). However, Fig. 8 shows that the chip / tool contact is above this range for v_c > 50m/min. The primary shear generates bulk chip temperatures in the range ≈ 250-300°C. The main plastic flow regions do not experience the blue-brittle condition.

However the situation changes as v_c falls below 50m/min. The chip / tool contact falls into the blue-brittle range. Fig. 9 shows the sensitivity of F_c* to *a* (the size of the blue-brittle peak, Eq. 3). There is a large sensitivity at v_c = 25-50m/min, an almost negligible sensitivity at 100m/min and no sensitivity at 150m/min. Bar charts of F_T* and *t/h* show the same trend. For *vc* ≤ 50m/min (when *h* = 0.3mm) the size of the blue-brittle peak must be considered, but built up edge forms at $v_c \leq$ 50m/min. Then damage modelling is also necessary [23].

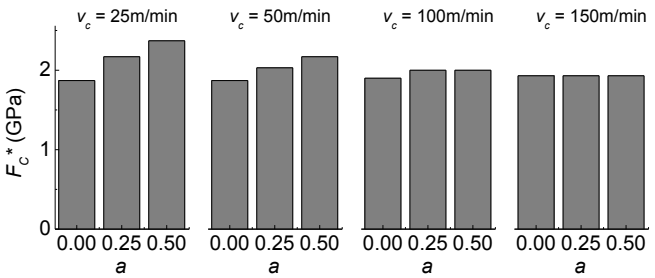

Fig. 9. Sensitivity of F_C* to *a* (Eq. 3) in the range 0 to 0.5, at cutting speeds v_c from 25 to 150m/min and *h* = 0.3mm.

The simulations behind Fig. 9 are with the same flow stress model as for Fig. 7, i.e. with the strain rate hardening increased above half the melting point (Eq. 5) and, in the case of Fig. 9, $m_0 = 0.03$. With $m_T = 0.0002$, m increases from 0.03 to 0.15 as T increases from 600 to 1200°C. This apparently small change has the same effect as previously was obtained by delaying thermal softening to 900°C (comparing Figs. 2 and 7). Changing m from 0.03 to 0.15 changes $g\left(\dot{\bar{\varepsilon}}\right)$ from 1.2 to 2.8 at the strain rate 10^3/s and from 1.3 to 4.0 at the strain rate 10^4/s. Inspection of Fig. 3 shows that these sizes of $g\left(\dot{\bar{\varepsilon}}\right)$ do indeed modify $\Theta(T)$ similarly to the previously supposed delayed thermal softening. Whether delayed softening or augmented hardening is physically more realistic remains an open question.

The previous delayed thermal softening and the present augmented strain rate hardening flow stress modifications change the flow stress at temperatures > 600-700°C; i.e. in the friction, shear, region next to the tool rake face. The present work's relevance to friction modelling is considered next.

5.2. Friction modelling

Simulations have been carried out, varying μ (Eq. 2) from 0 to 1. The predicted F_C and F_T have been resolved parallel and perpendicular to the rake face to obtain the friction and normal forces F_F and F_N. The nodal forces acting on the cutting edge radius, i.e. the ploughing forces, can be isolated with the software. Then F_F and F_N can be calculated both from the total forces and after subtracting the ploughing forces.

Fig. 10 shows the dependence of F_F/F_N on μ in two cases, $v_c = 100$ and 300m/min. In the 100m/min case, F_F/F_N is shown derived from both the total forces and without the ploughing forces. From total forces F_F/F_N has a non-zero intercept as μ reduces to zero. Without ploughing forces, $F_F/F_N = \mu$ below a critical value of μ. For higher μ F_F/F_N becomes constant. The transition corresponds to the friction law changing from $\tau = \mu\sigma_n$ to $\tau = k$. The critical value of μ for the transition is seen to be higher for $v_c = 100$m/min than for 300m/min.

Simulations have explored further how μ_{crit} varies with v_c from 50-150m/min, with h from 0.1-0.3 mm (with minimum mesh in proportion to h), and also with tool rake angle (γ = 6 or 0°) and tool thermal conductivity (K_{tool} = 40 or 100W/m°C).

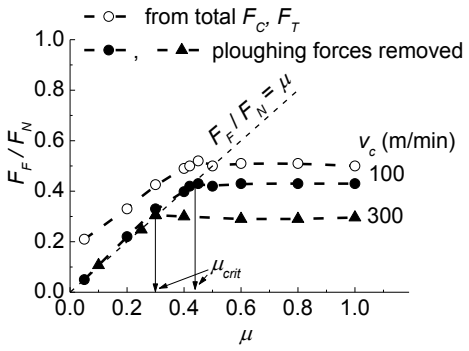

Fig. 10. Predicted F_F/F_N variation with μ for two examples, $v_c = 100$, 300 m/min, h = 0.3mm. F_F/F_N are obtained from both total F_C and F_T and after subtracting ploughing forces (Fig. 7 flow stress model, $m_0 = 0.03$).

Fig. 11 shows the dependence of μ_{crit} on v_c, for different values mainly of h but also of γ and K_{tool}. The dependence on γ and K_{tool} is minor within the range studied. The results for γ = 6° and K_{tool} = 40W/m°C are unified by plotting μ_{crit} against hv_c The solid lines in Fig. 11 are Eq. 7 (h *in* mm and v_c in m/min).

$$\mu_{crit} = 1.23\left(hv_c\right)^{-0.31} \tag{7}$$

hv_c unifies the results more successfully than does the physically plausible variable of rake face temperature. Fig. 13 shows a systematic influence of h in addition to temperature when μ_{crit} is plotted against average rake face temperature. It suggests that strain rate is also important.

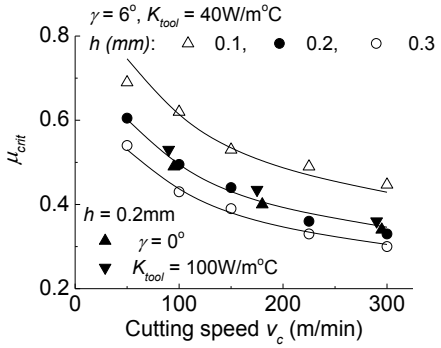

Fig. 11. μ_{crit} dependence on v_c, varying h, γ, K_{tool} (Fig. 10 flow stress model).

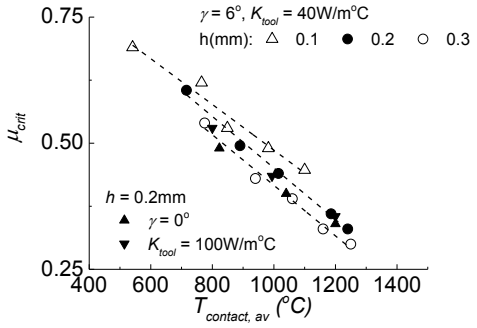

Fig. 12. μ_{crit} dependence on mean rake face contact temperature.

The trends of Figs.11, 12 show strong qualitative similarity to results from heavily loaded pin-on-disc and other tests that attempt to replicate the machining condition but without chip formation [10-12]. Particularly the range of μ from 0.3 to 0.7 is similar but the dependence on h (Fig. 11) and the size of temperature (Fig. 12) differ. These lead this author to believe that the machining test cannot be totally substituted.

However simulations which input a value of μ varying with v_c and h, rather than applying $\mu = 1$ as in the main part of this paper, can give good agreement with experimental forces and chip thicknesses. Applying μ_{crit} to the simulations in section 4 gives the same results as $\mu = 1$ (demonstrated in Fig. 10). An advantage of this approach is that the steel's high temperature flow stress behaviour becomes unimportant: when $\tau = \mu\sigma_n$ is active on the rake face there is no secondary shear. Fig. 13 illustrates this for a case when μ_{crit} = 0.43. In Fig.13a (μ = 0.45) there is a large rake face strain rate that is eliminated in Fig. 13b (μ = 0.40).

The values of μ from machining tests that relate to figures such as 11 are values after removing ploughing forces. Tests should therefore be carried out with tools of two different edge radii, to enable ploughing components to be determined. Then experimental laws such as Eq. 7 could be established. It would be of fundamental interest then to relate such laws back to flow stress models.

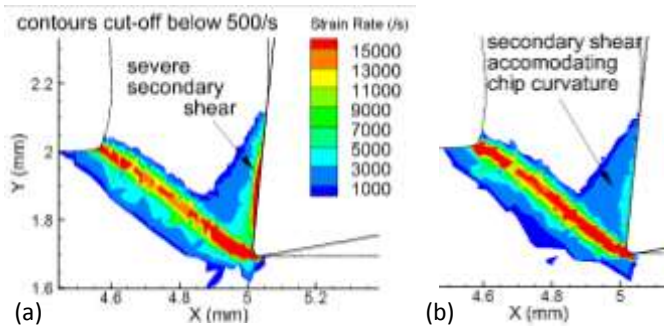

Fig. 13. Strain rate contours, h = 0.3mm, v_c = 100m/min: μ = (a) 0.45, (b) 0.4.

6. Conclusions

Flow stress models for annealed carbon and low alloy steels that are based on measurements of strain and strain rate hardening at room temperature and thermal softening at strain rates in the range 10^3-10^4/s need strain hardening to be adjusted for yield delay and either thermal softening to be delayed to 900°C or strain rate hardening to be augmented at temperatures > 600°C for accurate chip formation prediction. This is demonstrated here for machining a low alloy steel BS970:708M40, equivalent to AISI 4340. It is a change of view from that developed in [1-4] in which only thermal softening delay was considered.

The paper also considers the relationship between flow stress and chip/tool friction modelling. The description of chip /tool friction as depending on the chip shear stress under the local rake face conditions of temperature and strain rate can be replaced by a friction coefficient varying with cutting speed and uncut chip thickness but coefficients of the friction model should be obtained from cutting tests. It is of fundamental interest to integrate flow stress and friction modelling

Acknowledgements

I am grateful to members of the CIRP STC-C Cooperative Work on Material Constitutive Data and Models for Modelling of Metal Cutting, co-ordinated by Professor J. C. Outeiro (Arts et Metiers Paris Tech), for granting permission to include in section 2 data from their work on AISI 1045. In particular I wish to acknowledge that the data used in Figs. 3a and 4a have been generated by Professor Outeiro, Dr. A. Zabel (Technische Universitat Dortmund), Professor P.A.R. Rosa (University of Lisbon) and Professor F. Bleicher (TU Wien). I further wish to acknowledge that the ideas for the new material in this paper arose from lecture preparation in collaboration with Professor P-J Arrazola at Mondragon University.

This paper has not received any specific grant from funding agencies in the public, commercial or not-for-profit sectors for its original work.

References

[1] Childs THC.Modelling orthogonal machining of carbon steels. Part I: strain hardening and yield delay effects. International Journal of Mechanical Sciences 2009; 51; 402-411.

[2] Childs THC, Rahmad R. Modelling orthogonal machining of carbon steels. Part II: comparisons with experiments. International Journal of Mechanical Sciences 2009; 51; 465-472.

[3] Childs THC, Rahmad R. Modifying strain-hardening of carbon steels for improved finite element simulation of orthogonal machining. Journal of Engineering Manufacture 2009; 224Part B; 721-732.

[4] Childs THC, Otieno AW. Simulations and experiments on machining carbon and low alloy steels at rake face temperatures up to 1200°C. Machining Science and Technology 2012; 16; 96-110.

[5] Campbell JD. Dynamic plasticity: macroscopic and microscopic aspects. Materials Science and Engineering 1973; 12; 3-21.

[6]Zorev NN. Metal Cutting Mechanics, Pergamon Press, Oxford 1966, pp.279-281.

[7] Stevenson MG, Oxley PLG. An experimental investigation of the influence of strain rate and temperature on the flow stress properties of a low carbon steel using a machining test. Proceedings of the Institution of Mechanical Engineers 1970-71; 185; 741-754.

[8] Oyane M, Takashima F, Osakada K. The behaviour of steels under dynamic compression. In Proceedings 10th Japan Congress on Testing Materials – Mrtallic Materials, Kyoto 1967; 72-76.

[9] Hosford WF, Caddell RM. Metal Forming Mechanics and Metallurgy, Prentice-Hall, Englewood Cliffs NJ 1983, Fig. 5-3.

[10] Abdelali HB, Courbon C, Rech J. Identification of a friction model at the tool-chip-workpiece interface in dry machining of a AISI 1045 steel with a TiN coated carbide tool. J. Tribol. 2011; 133; 042201-1-11.

[11] Puls H, Klocke F, Lung D. Experimental investigation of friction under metal cutting conditions. Wear 2014; 310; 63-71.

[12] Zanger F, Bollig P, Schulze V. Simulative investigations on different friction coefficient models. Procedia CIRP 2017; 58; 140-145.

[13] Bleicher F, Outeiro JC, Rosa PAR, Zabel A. Private communication 2018 (see Acknowledgements).

[14] Shirakashi T, Maekawa K, Usui E. Flow stress of low carbon steel at high temperature and strain rate (Part 1) – propriety of incremental strain method in impact compression test with rapid heating and cooling systems. Bulletin JSPE 1983; 17; 161-166.

[15] Childs THC, Maekawa K. Computer-aided simulation and experimental studies of chip flow and tool wear in the turning of low alloy steels by cemented carbide tools. Wear 1990; 139; 235-250.

[16] Burns TJ, Mates SP, Rhorer RL, Whitenton EP, Basak D. Dynamic properties for modeling and simulation of machining: effect of pearlite to austenite phase transition on flow stress of AISI 1075 steel. Machining Science and Technology 2011; 15; 1-20.

[17] Jaspers SPFC, Dautzenberg JH. Material behaviour in conditions similar to metal cutting: flow stress in the primary shear zone. Journal of Materials Processing Technology 2002; 122; 322-330

[18] Johnson GR, Cook WH. A constitutive model and data for metals subjected to large strains, high strain rates and high temperatures. In Proc. 7th International Symposium on Ballistics, The Hague 1983; 541-547.

[19] Meyer LW, Herzig N, Halle T, Hahn F, Krueger L, Staudhammer KP. A basic approach for strain rate dependent energy conversion including heat transfer effects: an experimental and numerical study. Journal of Materials Processing Technology 2007; 182; 319-326.

[20] Singh NK, Cadoni E, Singha MK, Gupta NK. Dynamic tensile and compressive behaviours of mild steel at wide range of strain rates. Journal of Engineering Mechanics 2013; 139; 1197-1206.

[21] Langseth M. Lindholm US, Larsed PK, Lian B. Strain rate sensitivity of mild steel grade ST52-3N. Journal of Engineering Mechanics 1991; 117; 719-732.

[22] Zerilli FJ, Armstrong RW. Dislocation mechanics based constitutive relations for material dynamics calculations. Journal of Applied Physics 1987; 61; 1816-1825.

[23] Childs THC. Towards simulating built-up-edge formation in the machining of steel. CIRP Journal of Manufacturing Science and Engineering 2011; 4; 57-70.